Journal of
Synchrotron Radiation

ISSN 0909-0495

Received 18 December 2012
Accepted 5 July 2013

Periodically structured X-ray waveguides

Inna Bukreeva,[a]* Andrea Sorrentino,[a,b] Alessia Cedola,[a] Ennio Giovine,[a] Ana Diaz,[c] Fernando Scarinci,[a] Werner Jark,[d] Leonid Ognev[e] and Stefano Lagomarsino[f,g]

[a]Institute for Photonics and Nanotechnologies, CNR, 00156 Rome, Italy, [b]ALBA Synchrotron Light Source, Cerdanyola del Valles, 08290 Barcelona, Spain, [c]Paul Scherrer Institut, CH-5232 Villigen PSI, Switzerland, [d]Elettra, Sincrotrone Trieste, 34149 Basovizza, Trieste, Italy, [e]Kurchatov Institute, NRC, Moscow 123182, Russian Federation, [f]Institute for Chemical-Physical Processes, CNR, 00185 Rome, Italy, and [g]Physics Department, Sapienza University, 00185 Rome, Italy.
E-mail: innabukreeva@yahoo.it

The properties of X-ray vacuum-gap waveguides (WGs) with additional periodic structure on one of the reflecting walls are studied. Theoretical considerations, numerical simulations and experimental results confirm that the periodic structure imposes additional conditions on efficient propagation of the electromagnetic field along the WGs. The transmission is maximum for guided modes that possess sufficient phase synchronism with the periodic structure (here called 'super-resonances'). The field inside the WGs is essentially given at low incidence angle by the fundamental mode strongly coupled with the corresponding phased-matched mode. Both the simulated and the experimental diffraction patterns show in the far field that propagation takes place essentially only for low incidence angles, confirming the mode filtering properties of the structured X-ray waveguides.

Keywords: X-ray beams and X-ray optics; synchrotron radiation instrumentation; X-ray microscopes; wave propagation; transmission and absorption; interference.

1. Introduction

The propagation of modes in waveguides (WGs) with gratings is a topic of considerable interest. In particular, waveguides with additional periodicity have been extensively explored for visible light and microwaves for over half a century and find many applications in integrated optics (Yariv & Nakamura, 1977; Conwell, 1976). On the other hand, X-ray waveguides, developed in the mid-1990s, are a relatively recent contribution to the field of optics. WGs are able to provide sub-micrometer coherent X-ray beams in a large energy range, both in one and two dimensions (Lagomarsino *et al.*, 1996; Feng *et al.*, 1995; Pfeiffer *et al.*, 2002). They have been applied recently to X-ray microscopy, holography and coherent diffraction imaging (Giewekemeyer *et al.*, 2010; De Caro *et al.*, 2008; Pelliccia *et al.*, 2010) at both synchrotron and laboratory sources. Each resonance mode propagating inside the WG has a well defined wavefront (Bukreeva *et al.*, 2010; Zwanenburg *et al.*, 1999). However, in the front coupling geometry (Zwanenburg *et al.*, 1999; Pelliccia *et al.*, 2007), several modes are generally excited simultaneously, and the resulting wavefront can thus be rather complex. Moreover, the degree of coherence is conditioned by the coherence at the WG entrance. Analysis of coherence properties and filtering of X-ray beams in WGs can be performed by averaging of radiation from several points (Osterhoff & Salditt, 2011). Fabrication of single-mode X-ray WGs and reconstruction of exit fields was discussed by Krüger *et al.* (2012).

In a recent paper, Bukreeva *et al.* (2011) demonstrated theoretically that an additional symmetric periodic structure on the reflecting walls of a WG with a gap of a few hundred nanometers can filter out the asymmetric and the high-order modes. Then the WG can provide a highly coherent exit beam, even with partially coherent illumination. A recent theoretical and experimental investigation of the vertical multilayer B_4C/Al_2O_3 periodic structure within WGs also demonstrated resonant single-mode propagation of X-rays (Okamoto *et al.*, 2012).

In this paper we present both theoretical and experimental studies of the properties of structured X-ray WGs, in particular of the mode filtering effect. This paper is organized as follows: the theoretical analysis and computer simulations of electromagnetic field propagation in structured WGs are given in §2; experimental results, obtained at the cSAXS beamline at the Swiss Light Source, are reported in §3; a general discussion and the conclusions are provided in §4.

2. Guided-mode propagation analysis in structured WGs

Let us consider a structured WG, schematically shown in Fig. 1, in which the periodic structure (a reflecting grating with

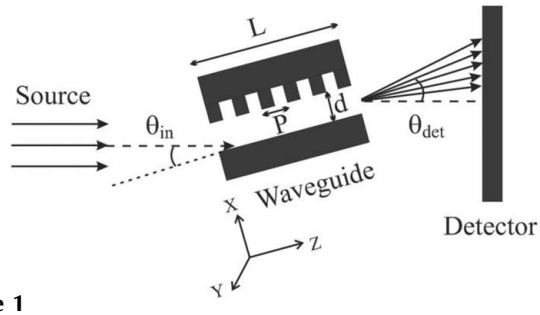

Figure 1
Sketch of a structured X-ray waveguide with only one side structured with a grating. The incoming X-rays impinge on the WG at an angle θ_{in}. L is the WG length, d is the gap value and P is the grating period. θ_{det} are the diffraction angles measured with respect to the incident beam.

Ronchi ruling with a period of about $P = 200$ µm, a duty cycle of 1/2 and a depth of $A = 6$ µm) has been created on only one of the two reflecting sidewalls of the WG. The material constituting the walls is silicon with refraction index $n_0 = \varepsilon^{1/2} = 1 - \delta + i\beta$. From Henke *et al.* (1993) we obtain $\delta = 7.6733 \times 10^{-6}$ and $\beta = 1.7688 \times 10^{-7}$ at the photon energy of 8 keV considered here. In the coordinate system shown in Fig. 1 the axis $0Z$ is parallel to the vacuum-slab boundary of the waveguide, and the axis $0X$ is along the WG gap. The waveguide, whose channel length is 4 mm, is illuminated in front coupling geometry by a plane wave. Since the transverse dimension of the guiding layer (the gap) is much smaller than the lateral one (along axis $0Y$), the problem of X-ray propagation in the section has been treated two-dimensionally.

We present initially the basic equations for uniform (*i.e.* non-structured) WGs, which are well known in the literature (Marcuse, 1974), and then we will extend the analysis to structured WGs.

2.1. X-ray propagation in a uniform waveguide

Assuming the small value of reflection, diffraction and scattering angles mainly contributing to the transmitted beam [$\theta < \theta_c = (2\delta)^{1/2} \simeq 10^{-3}$ rad] and using the paraxial approximation for the electric field $E = \Psi(x, z)\exp(ikz)$, the slowly changing amplitude $\Psi(x, z)$ is given as the solution of the parabolic wave equations (PWEs),

$$2ik\,\partial\Psi/\partial z = \Delta_\perp\Psi + k^2(\varepsilon - 1)\Psi, \tag{1}$$

where $\varepsilon(x)$ is the permittivity of the material, which changes abruptly at the vacuum–material boundaries. At a distance z from the entrance of the multimodal waveguide the wave amplitude with input profile $\Psi(x, z = 0)$ can be written as a superposition of modes $\psi_m(x)$,

$$\Psi(x, z) = \sum_m c_m\psi_m(x)\exp\left(-ik_{zm}z - \gamma_m z\right), \tag{2}$$

where $m = 0, 1, 2, \ldots$ is the mode number, γ_m is the mode damping coefficient, k_{zm} is the 'slow' longitudinal wavevector for the mth mode, and c_m is the excitation coefficient for mode m.

Within the coordinate system depicted in Fig. 1, the modes can be chosen inside the channel in the form (Ognev, 2010)

$$\psi_m(x) = \sin(q_{xm}x - \varphi_m), \tag{3}$$

where $q_{xm}^2 = -k(2k_{zm})$ and q_{xm} can be regarded as the projection of the wavevector $\mathbf{k}$ on the lateral axis $0X$ for the m mode. The phase term φ_m in (3) is given by

$$\varphi_m = \arcsin(q_{xm}/k\theta_c) + \pi(m + 1), \tag{4}$$

where m is an integer and $\theta_c = [\mathrm{Re}(1 - \varepsilon_0)]^{1/2}$ is the Fresnel critical angle for total external reflection.

The phase term in (4) takes into account the penetration of the electromagnetic field into the cladding material which causes effective broadening of the geometrical width d of the guiding layer. For angles much less than the critical angle, $q_{xm}/k\theta_c \ll 1$, the waveguide dispersion equation can be expressed in a simple form,

$$q_{xm} = \pi(m + 1)/d_{\mathrm{eff}}, \tag{5}$$

where the effective width of the guiding layer is $d_{\mathrm{eff}} \simeq d + \lambda/\pi\theta_c$. For X-ray radiation with photon energy 8 keV and a Si substrate the effective guiding layer broadening is $\lambda/\pi\theta_c \simeq 12.6$ nm. Since θ_c is proportional to λ, in this approximation d_{eff} is independent of the photon energy.

Taking into account (5), the longitudinal wavenumber k_{zm} is given by

$$k_{zm} = -q_{xm}^2/2k = -2\pi(m + 1)^2/z_T, \tag{6}$$

where z_T is the self-imaging or Talbot distance for the waveguide (Bukreeva *et al.*, 2011),

$$z_T = 2(2d_{\mathrm{eff}})^2/\lambda. \tag{7}$$

2.2. X-ray propagation in structured waveguides

Mathematically the physical processes that occur in a periodic waveguide have been treated either with the guide modes as sums of Bloch–Floquet waves (Peng *et al.*, 1974; Peng *et al.*, 1975) or as a solution of the coupled-wave equations (Yariv & Nakamura, 1977; Conwell, 1976; Marcuse, 1969). To solve coupled-wave equations one can usually make some simplifying assumptions. A very common and usually good assumption in optical WGs is that the interaction between two given modes is particularly strong. In the following we will demonstrate using computer simulations that also in the X-ray region the propagation in a structured WG can cause coupling between two strongly interacting modes. We used two different computer codes based on the solution of the parabolic wave equation. The first one is based on the finite differences method (Kopylov *et al.*, 1995); the second is based on a splitting scheme (Ognev, 2002) with a successive calculation of diffraction and the phase change at each step. Both methods gave identical results. The X-ray optical properties for silicon were taken from Henke *et al.* (1993).

To study the propagation of the electromagnetic field in structured WGs we started from the assumption that the angular spectrum of the transmitted wavefield has to satisfy the resonance conditions determined by two main factors. The first is related to the periodicity of the wavefield in the

waveguide; the second is connected to the periodicity of the reflection grating. In general, the two periodicities do not match each other.

The frequency spacing between two guided modes, taking into account (6), can be written as

$$k_{zl} - k_{zm} = -\frac{q_{xm}^2 - q_{xl}^2}{2k} = 2\pi\frac{(m+1)^2 - (l+1)^2}{z_T}. \quad (8)$$

Therefore the longitudinal period of the wavefield modulation or mode beating between the mode m and mode l in the guiding layer is given by

$$T = \frac{z_T}{(m+1)^2 - (l+1)^2}. \quad (9)$$

The modes will be coupled and propagate efficiently in the WG only when the periodicity of the beating T [equation (9)] matches the periodicity P imposed by the grating, $k_{zl} - k_{zm} = (2\pi/P)n$, or in other words when

$$P = nT = \frac{z_T}{(m+1)^2 - (l+1)^2}\, n, \quad (10)$$

where $n = \pm 1, \pm 2, \ldots$ are the Fourier harmonics of the grating. Equation (10) is known as the Bragg condition or the longitudinal phase matching for the guided modes which hereinafter we will call 'super-resonance'. Furthermore, we restrict ourselves to the consideration of exclusively co-directional interactions between two forward propagating modes because, contrary to the optical case, the amplitude of the backward running mode is negligibly small for X-ray radiation. When the phase-matching condition, equation (10), is not fulfilled (*i.e.* when $P \neq T$), the propagation field is rapidly damped along the guiding layer. Therefore, for an efficient propagation according to (10), either the grating periodicity has to be chosen appropriately, or the WG gap needs to be properly adjusted.

With symmetric illumination of the WG (zero grazing-incidence angle θ_{in}; see Fig. 1), the interference pattern in the guiding layer is characterized by the beating of the fundamental mode $l = 0$ with the corresponding resonance mode m. The lateral dimension of the vacuum gap which provides the phase matching of the selected modes can be found from (10) with $n = 1$ (Yariv & Nakamura, 1977),

$$d_{\rm eff} = (1/2)\left\{\lambda\left[(m+1)^2 - 1\right]P/2\right\}^{1/2}. \quad (11)$$

Taking the grating period $P = 200$ µm, one can obtain from (11) the vacuum guiding layer widths which satisfy the longitudinal phase-matching conditions: $d_{\rm eff} = 108$ nm ($m = 1$), $d_{\rm eff} = 176$ nm ($m = 2$), $d_{\rm eff} = 241$ nm ($m = 3$), $d_{\rm eff} = 305$ nm ($m = 4$).

In Fig. 2(*a*) we show the super-resonance effect, plotting the transmission calculated numerically as a function of the effective vacuum gap width $d_{\rm eff}$, for the structured WG (solid line), compared with the transmission coefficient for a uniform waveguide (dashed line). For the structured WG, sharp super-resonance maxima occur for the guiding layer dimensions corresponding to equation (11). The structured waveguide transmits less energy compared with the uniform waveguide

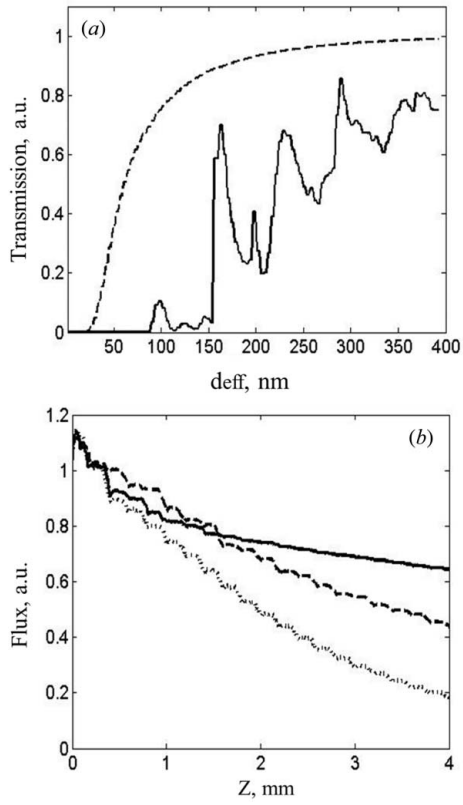

Figure 2
(*a*) Simulated transmission coefficient for the uniform (non-structured) WG (dashed line) and for the structured WG (solid line) as a function of the effective transverse dimension of the guiding layer. (*b*) Flux attenuation along the structured waveguide with vacuum gap $d_{\rm eff}$ = 241 nm (solid line) corresponding to super-resonance conditions $d_{\rm eff}$ = 225 nm (dotted line), $d_{\rm eff}$ = 280 nm (dashed line). In the calculation the incident photon energy was $E_{\rm inc} = 8$ keV, the WG length $L = 4$ mm and the grating period $P = 200$ µm.

owing to the strong attenuation of modes which do not satisfy the phase-matching condition. In Fig. 2(*b*) we show the field attenuation along the WG for the gap $d_{\rm eff} = 241$ nm matching the super-resonance conditions (black line) and for gaps just below ($d_{\rm eff} = 225$ nm, dotted line) and just above ($d_{\rm eff} = 280$ nm, dashed line) the first one. As expected, the latter two are damped more significantly along the guiding length. To demonstrate that under super-resonance conditions mainly two coupled modes propagate, we show in Figs. 3(*a*)–3(*d*) the intensity distribution in the structured waveguide at symmetric illumination in the case when the phase-matching condition of (11) is satisfied for the modes with numbers $m = 1$ (Fig. 3*a*), $m = 2$ (Fig. 3*b*), $m = 3$ (Fig. 3*c*) and $m = 4$ (Fig. 3*d*).

Qualitative modal structure analysis in the WG is performed with the Fourier transform of the field with respect to the $0Z$ axis far from the WG entrance, where the modes out of the super-resonance conditions are damped out. This method was earlier applied to X-ray waveguides and electron channelling (Fuhse & Salditt, 2005; Dabagov & Ognev, 1988). The modulus of the Fourier transform is shown in Figs. 3(*e*) to 3(*h*) for $m = 1$, $m = 2$, $m = 3$ and $m = 4$.

From Fig. 3 one can see that the structured WG transmits mostly the fundamental mode and the mode m selected with

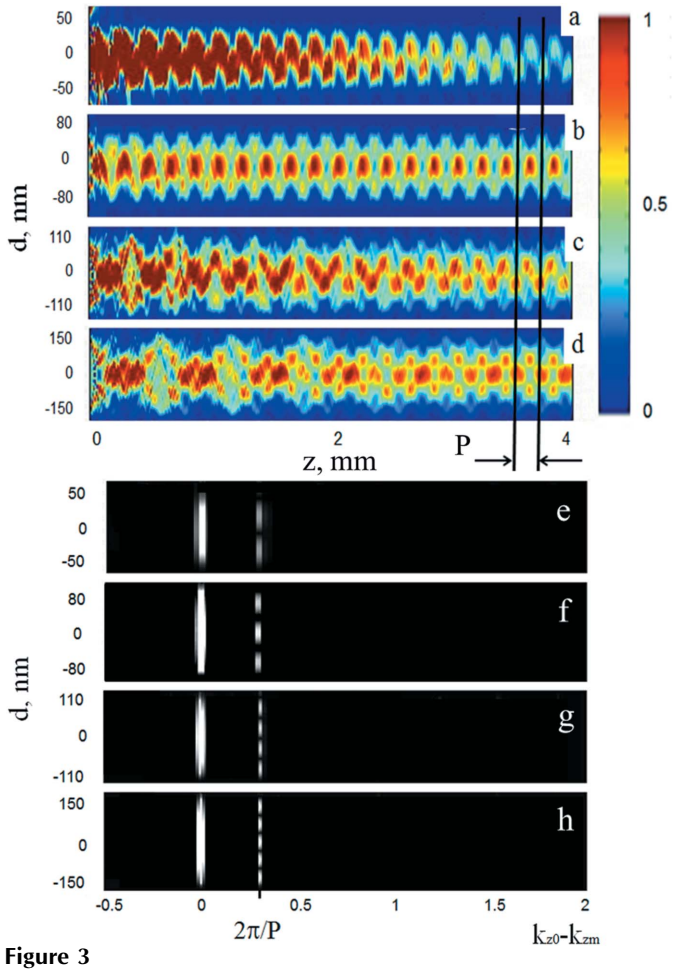

Figure 3
Top: interference pattern given by modes propagating in the guiding layer with lateral dimensions $d_{\rm eff}$ equal to (*a*) 108 nm, (*b*) 176 nm, (*c*) 241 nm, (*d*) 305 nm. The color bar indicates intensity in a.u. Bottom: modal structure of the field propagated in the WG found as a Fourier transform of the field with respect to the optical axis of the waveguide (axis 0*Z*) for the same vacuum gaps: (*e*) 108 nm, (*f*) 176 nm, (*g*) 241 nm, (*h*) 305 nm. As in the previous figure the incident photon energy was $E_{\rm inc}$ = 8 keV, the WG length L = 4 mm and the grating period P = 200 µm

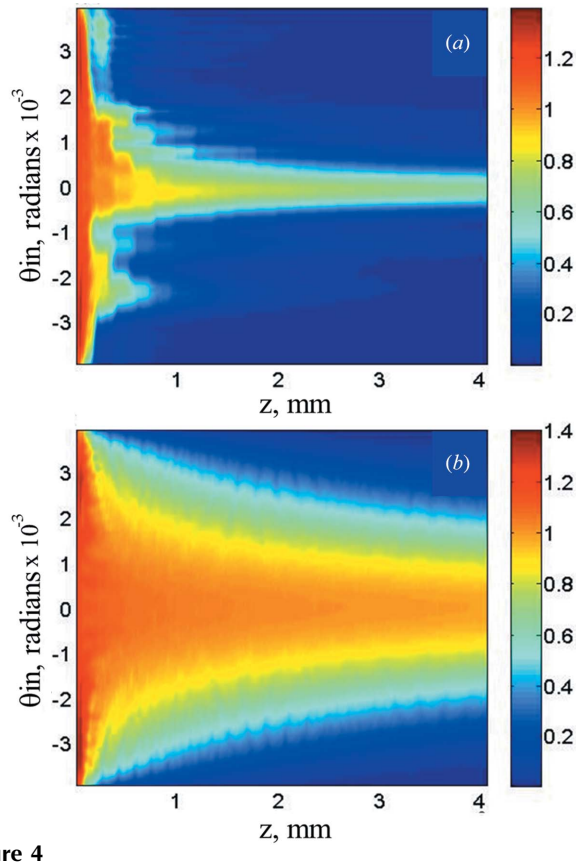

Figure 4
Variation along the WG of the intensity integrated over the channel width, normalized to the incident integrated intensity, for different incident angles $\theta_{\rm in}$, in (*a*) the structured WG, (*b*) the uniform WG. In both cases the vacuum gap was $d_{\rm eff}$ = 241 nm and the incident energy was 8 keV. The period P in the structured WG was 200 µm. The figure clearly shows selective transmission for the structured WG.

equation (11). Under these conditions the interference pattern is characterized by the beating of the fundamental mode with the corresponding resonance mode m = 1 at $d_{\rm eff}$ = 108 nm [Figs. 3(*a*) and 3(*e*)], m = 2 at $d_{\rm eff}$ = 176 nm [Figs. 3(*b*) and 3(*f*)], m = 3 at $d_{\rm eff}$ = 242 nm [Figs. 3(*c*) and 3(*g*)] and m = 4 at $d_{\rm eff}$ = 305 nm [Figs. 3(*d*) and 3(*h*)], for the given period P = 200 µm of the grating.

Different from the uniform waveguide, which at symmetric illumination ($\theta_{\rm in}$ = 0) propagates only symmetric modes, the structured waveguide can propagate both symmetric and asymmetric modes.

The filtering properties of the structured WG of high-order modes are shown in Fig. 4, where we report the X-ray flux attenuation in the structured (*a*) and uniform (*b*) waveguide with resonance vacuum gap $d_{\rm eff}$ = 241 nm at different angles $\theta_{\rm in}$ of the waveguide illumination. It follows from the figure that the transmission in the structured waveguide is essentially limited to small incident angles, and that effective mode filtering takes place with respect to uniform WGs. A slight increase of X-ray beam transmission at the negative angle $\theta_{\rm in} \simeq 2.2$ mrad in Fig. 4(*a*) corresponds to the phase matching of high-order modes with l = 6 and m = 7 [see equation (10)]. However, one can see from the figure that the structured waveguide effectively suppresses these high-order coupled modes excited at angles different from zero.

Simulation for structured WGs with different groove depths has shown that the transmission of X-rays does not depend on groove depth if this exceeds the gap value.

3. Experiment

3.1. WG fabrication

The WG was made from two silicon slabs, 8 mm × 4 mm; in one of them an empty channel was obtained by depositing a Cr layer with thickness equal to the desired WG gap (240 nm in our case) on the entire surface, except for a central channel, approximately 1 mm wide. The other silicon slab, of the same dimensions as the first one, but without the Cr spacer, was positioned on the first one in such a way as to have a perfect superposition. The two slabs were held firmly, one against the other, with the aid of a mechanical press (Fig. 5*a*) (Pelliccia *et al.*, 2007).

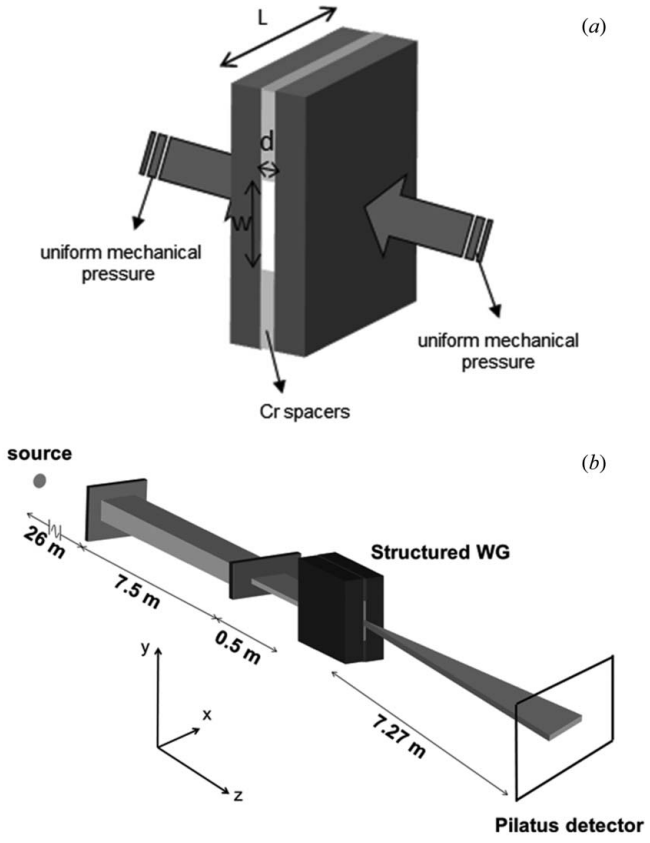

Figure 5
(*a*) Schematic picture of the WG with air gap. Two 4 mm × 8 mm Si slabs were firmly pressed one against the other. One slab has two Cr shoulders, about 200 nm thick, which leave one free channel with one nanometric dimension d corresponding to the WG gap, and one macroscopic dimension w (in this case ∼1 mm); one slab had in addition a periodic structure with period P = 200 µm along the WG length L (see Fig. 1). (*b*) Experimental set-up assembled at the cSAXS beamline for testing the structured WG. The beam was defined by two slit systems, defining a beam at the WG entrance of about 0.6 mm (H) × 0.1 mm (V), with a divergence of about 18 µrad (H) × 3 µrad (V).

In the case of the structured WG, the periodic grating was fabricated directly on the silicon slab with the Cr shoulders, using electron beam lithography (Vistec EPBG5 High Resolution, acceleration voltage 100 keV) and silicon etching. A 1.4 µm-thick layer of a positive-tone electronic resist, polymethyl methacrylate (PMMA), 600k molecular weight, was spun on the silicon top layer and baked at 442 K for 5 min on a hotplate, exposed with a dose of 800 µC cm^{-2}, and developed with a methyl isobutyl ketone and isopropyl alcohol (1:1 solution) for 90 s. The pattern was then transferred into the substrate by means of an inductively coupled plasma (ICP) system, using a two-step process for Si etching. In the first step a plasma containing C_4F_8 (30 sccm; sccm = standard cubic centimeters per minute) and Ar (187 sccm) gases, at 70 mtorr pressure and 600 W RF power (t = 2 s), was used to passivate the walls of the trench; in the second step the etching was performed by Ar (100 sccm) and SF_6 (130 sccm) gases, at 30 mtorr pressure and 500 W RF power for t = 10 s. The silicon grating height was 6 µm, obtained in six steps of the ICP process.

3.2. Experimental set-up

The experiment was carried out at the cSAXS beamline at the Swiss Light Source, Villigen, Switzerland, using the set-up shown in Fig. 5(*b*).

We used the X-ray undulator beam monochromated at 8 keV photon energy by a fixed-exit Si(111) monochromator. The total distance between the source and the WG entrance was 34 m. The beam size was firstly defined by a pair of slits at 26 m from the source to 0.5 mm in the vertical (y) direction and 0.6 mm in the horizontal (x) direction. In addition, a third slit placed at 33.5 m from the source further reduced the beam size in the vertical direction to 0.1 mm. This slits setting gives a final divergence on the WG entrance plane of 18 µrad on the horizontal and 3 µrad on the vertical direction. No prefocusing optics was used. The photon flux was estimated to be 1.6×10^{11} photons s^{-1} spread over a 0.6 mm × 0.1 mm area, corresponding to a flux density of 2.7×10^{12} photons mm^{-2}. The WG was mounted on a hexapod (http://www.hexapods.net/) allowing six degrees of freedom for careful orientation of the waveguide with respect to the incident beam. The WG entrance was first centered on the beam using the x and y translations taking care that its reflecting surface is in the yz plane, and then the different incident angles were selected rotating the WG around the y axis. A PILATUS 2M detector (Kraft *et al.*, 2009) with pixel size of 172 µm was placed downstream of the WG at a distance of 7.27 m. A He-filled flight tube between the WG and the detector reduced air scattering and absorption.

3.3. Experimental results

The scope of the experiment was to measure the intensity distribution provided by the structured WG as a function of the incident angle, and to compare the experimental results with simulations based on the equations reported in §2.2. To this purpose the far-field diffraction pattern has been recorded for a given range of incident angles. The WG was rotated in steps of 0.0025° over a total range of 0.6°, slightly exceeding double the critical angle θ_c, and at each step an image was recorded at the detector with an exposure time of 1 s for a total scanning time of ∼4 min. Fig. 6(*a*) shows a representative far-field pattern, obtained for a small grazing incidence angle θ_{in} (rotation around the y axis) corresponding to the maximum intensity at the detector. The WG reflecting surfaces are in the yz plane (see Fig. 5*b*); consequently in the vertical direction the beam maintains its natural divergence, but in the horizontal direction the beam acquires a divergence α owing to diffraction at the exit of the WG. Fig. 6(*b*) shows the beam profile along the x direction, obtained by integrating the intensity along 21 pixels in the y direction. The same procedure was repeated for all the images, each one corresponding to a given incidence angle, and the two-dimensional intensity distribution $I(\theta_{in}, \theta_{det})$ shown in Fig. 7(*a*) was eventually obtained, where the abscissa θ_{in} is the grazing-incidence angle of the incoming beam and the ordinate θ_{det} is the exit angle of radiation with respect to the incident direction (see Fig. 1). Fig. 7(*b*) shows the corresponding computer simulation

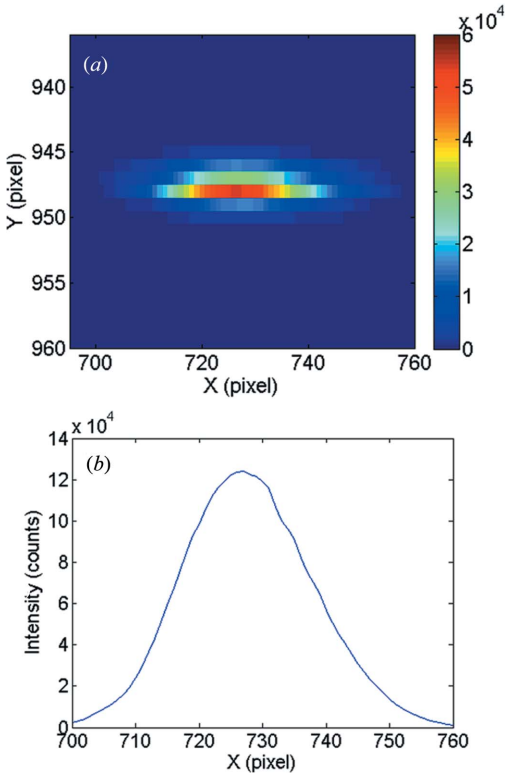

Figure 6
(*a*) Far-field pattern for one angular position of the WG. The intensity in arbitrary units is given in gray scale (color in the on-line version) as a function of the detector pixel in the X (horizontal) and Y (vertical) directions. Along X the beam acquires a divergence of the order of λ/d because of diffraction at the exit of the WG. In the y direction the beam maintains its natural divergence of about 3 µrad. (*b*) Beam profile in the horizontal direction obtained by integrating the intensity distribution in (*a*) for 21 pixels along y. From the measure of the cross-section width it is possible to roughly derive the gap value d, resulting in about 240 nm.

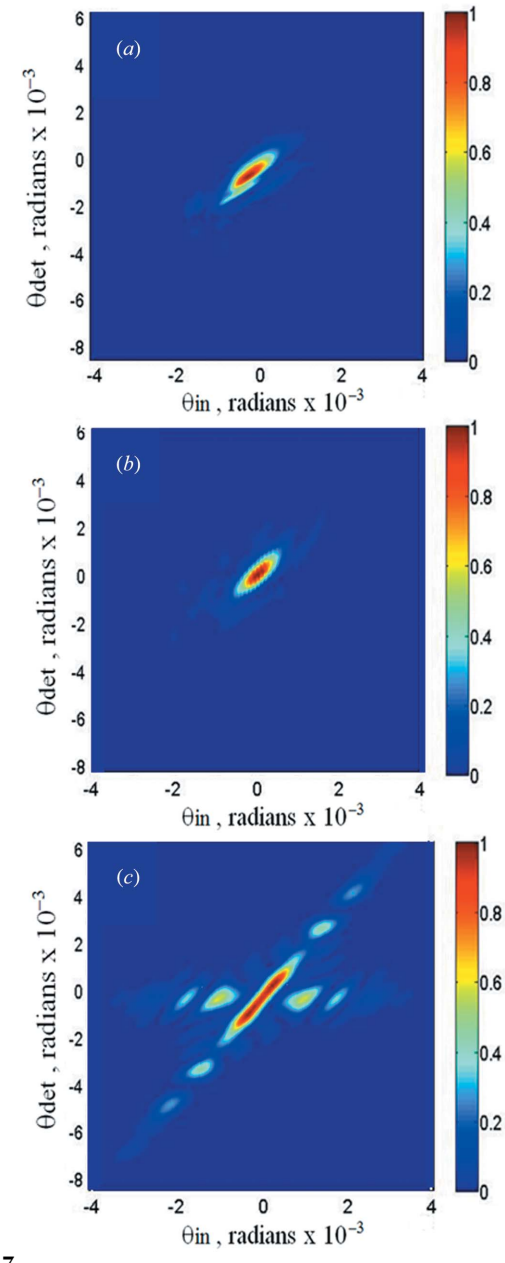

Figure 7
Comparison between experimental results and computer simulations. All the figures show the intensity distribution $I(\theta_{in}, \theta_{det})$ (see text and Fig. 1). (*a*) Experimental results. (*b*) Simulated pattern for a structured WG with grating period P = 200 µm. (*c*) Simulated pattern for a uniform WG. In (*b*) and (*c*) we considered the effective gap value d_{eff} = 241 nm and the incident energy E = 8 keV.

calculated for a structured waveguide with vacuum gap d_{eff} = 241 nm, grating period P = 200 µm and energy 8 keV, the same as that used in the experiment. The agreement is very good, and confirms that the structured WG indeed has an efficient transmission only for low grazing incidence angles. For comparison, Fig. 7(*c*) reports the same type of image $I(\theta_{in}, \theta_{det})$ calculated for a uniform WG with the same gap value of 241 nm. In this case several resonance modes are visible, with detectable intensity in the entire angular range up to the critical angle θ_c.

4. Conclusions

The properties of X-ray vacuum-gap WGs with an additional periodic structure on the reflecting walls have been investigated. We demonstrated using computer simulation that efficient propagation of X-ray radiation in a vacuum gap of a few hundred nanometers takes place when resonance modes are phase matched with the periodicity imposed by the grating. In particular, at small grazing incidence angle, the electromagnetic wavefield inside the WG is given by the interference between the fundamental mode and one of the modes with number m = 1, m = 2, m = 3 and m = 4. Consequently, superresonance conditions are satisfied, for a given periodicity, only for well determined values of the effective WG gap d_{eff}, where d_{eff} includes the geometrical gap and the penetration depth in the cladding layers. When these conditions are not fulfilled, the attenuation of the electromagnetic wavefield along the structured WG is stronger. On the other hand, simulations show that detectable transmission will be observed only close to zero incidence angle. Experimental results taken with synchrotron radiation confirm the theoretical findings with a good agreement between the experimental and simulated far-field diffraction patterns.

Structured WGs can find applications in all the cases when a coherent and well defined wavefront has to be obtained. In particular, when laboratory sources or synchrotron radiation beamlines with pre-focusing optics are used, the wavefront can be quite different from a plane wave. The structured WG, different with respect to a pinhole or to a uniform WG, will transmit only X-ray radiation in a narrow angular range, providing at its exit a well defined wavefront.

We thank Andreas Menzel for his comments on the manuscript and Xavier Donath for technical support during the measurements. One of the authors (LO) was partially supported by grant No. 4361.2012.2 from the President of Russian Federation for Leading Scientific Schools.

References

Bukreeva, I., Cedola, A., Sorrentino, A., Pelliccia, D., Asadchikov, V. & Lagomarsino, S. (2011). *Opt. Lett.* **36**, 2602–2604.
Bukreeva, I., Pelliccia, D., Cedola, A., Scarinci, F., Ilie, M., Giannini, C., De Caro, L. & Lagomarsino, S. (2010). *J. Synchrotron Rad.* **17**, 61–68.
Conwell, M. (1976). *Phys. Today*, **29**, 48–59.
Dabagov, S. B. & Ognev, L. I. (1988). *Nucl. Instrum. Methods Phys. Res. B*, **30**, 185–190.
De Caro, L., Giannini, C., Pelliccia, D., Mocuta, C., Metzger, T. H., Guagliardi, A., Cedola, A., Burkeeva, I. & Lagomarsino, S. (2008). *Phys. Rev. B*, **77**, 081408.
Feng, Y. P., Sinha, S. K., Fullerton, E. E., Grübel, G., Abernathy, D., Siddons, D. P. & Hastings, J. B. (1995). *Appl. Phys. Lett.* **67**, 3647.
Fuhse, C. & Salditt, T. (2005). *Physica B*, **357**, 57–60.
Giewekemeyer, K., Neubauer, H., Kalbfleisch, S., Krüger, S. P. & Salditt, T. (2010). *New J. Phys.* **12**, 035008.
Henke, B. L., Gullikson, E. M. & Davis, J. C. (1993). *At. Data Nucl. Data Tables*, **54**, 181–342.
Kopylov, Y. V., Popov, A. V. & Vinogradov, A. V. (1995). *Opt. Commun.* **118**, 619–636.
Kraft, P., Bergamaschi, A., Broennimann, Ch., Dinapoli, R., Eikenberry, E. F., Henrich, B., Johnson, I., Mozzanica, A., Schlepütz, C. M., Willmott, P. R. & Schmitt, B. (2009). *J. Synchrotron Rad.* **16**, 368–375.
Krüger, S. P., Neubauer, H., Bartels, M., Kalbfleisch, S., Giewekemeyer, K., Wilbrandt, P. J., Sprung, M. & Salditt, T. (2012). *J. Synchrotron Rad.* **19**, 227–236.
Lagomarsino, S., Jark, W., Di Fonzo, S., Cedola, A., Mueller, B., Engström, P. & Riekel, C. (1996). *J. Appl. Phys.* **79**, 4471.
Marcuse, D. (1969). *Bell Syst. Tech. J.* **48**, 3187–3215.
Marcuse, D. (1974). *Theory of Dielectric Optical Waveguides.* New York: Academic Press.
Ognev, L. I. (2002). *X-ray Spectrom.* **31**, 274–277.
Ognev, L. I. (2010). *Tech. Phys.* **55**, 1628–1632.
Okamoto, K., Noma, T., Komoto, A., Kubo, W., Takahashi, M., Iida, A. & Miyata, H. (2012). *Phys. Rev. Lett.* **109**, 233907.
Osterhoff, M. & Salditt, T. (2011). *New J. Phys.* **13**, 103026.
Pelliccia, D., Bukreeva, I., Ilie, M., Jark, W., Cedola, A., Scarinci, F. & Lagomarsino, S. (2007). *Spectrochim. Acta B*, **62**, 615–621.
Pelliccia, D., Sorrentino, A., Bukreeva, I., Cedola, A., Scarinci, F., Ilie, M., Gerardino, A. M., Fratini, M. & Lagomarsino, S. (2010). *Opt. Express*, **18**, 15998–16004.
Peng, S. T., Bertoni, H. L. & Tamir, T. (1974). *Opt. Commun.* **10**, 91–94.
Peng, S. T., Tamir, T. & Bertoni, H. L. (1975). *IEEE Trans. Microw. Theory Tech.* **23**, 123–133.
Pfeiffer, F., David, C., Burghammer, M., Riekel, C. & Salditt, T. (2002). *Science*, **12**, 230–234.
Yariv, A. & Nakamura, M. (1977). *IEEE J. Quantum Electron.* QE-**13**, 233–253.
Zwanenburg, M. J., Peters, J. F., Bongaerts, J. H. H., de Vries, S. A., Abernathy, D. L. & van der Veen, J. F. (1999). *Phys. Rev. Lett.* **82**, 1696–1699.